

## Automation and Experience of Controlled Crystal Dehydration: Results from the European Synchrotron HC1 Collaboration

Matthew W. Bowler,<sup>\*,†,‡</sup> Uwe Mueller,<sup>§</sup> Manfred S. Weiss,<sup>§</sup> Juan Sanchez-Weatherby,<sup>||</sup>  
Thomas L-M. Sorensen,<sup>||</sup> Marjolein M. G. M. Thunnissen,<sup>⊥,♯</sup> Thomas Ursby,<sup>⊥</sup> Alexandre Gobbo,<sup>†,‡</sup>  
Silvia Russi,<sup>†,‡,◆</sup> Michael G. Bowler,<sup>▽</sup> Sandor Brockhauser,<sup>†,‡</sup> Olof Svensson,<sup>○</sup> and Florent Cipriani<sup>\*,†,‡</sup>

<sup>†</sup>European Molecular Biology Laboratory, Grenoble Outstation, 71 avenue des Martyrs, CS 90181, F-38042 Grenoble, France

<sup>‡</sup>Unit for Virus Host Cell Interactions, Université Grenoble Alpes-EMBL-CNRS, 71 avenue des Martyrs, CS 90181, F-38042 Grenoble, France

<sup>§</sup>Macromolecular Crystallography (HZB-MX), Helmholtz-Zentrum Berlin, F-ISFM, Albert-Einstein-Strasse 15, D-12489 Berlin, Germany

<sup>||</sup>Diamond Light Source Ltd., Harwell Science and Innovation Campus RAL, Chilton, Didcot OX11 0DE, U.K.

<sup>⊥</sup>The MAX IV Laboratory, Lund University, P. O. Box 118, SE-22100 Lund, Sweden

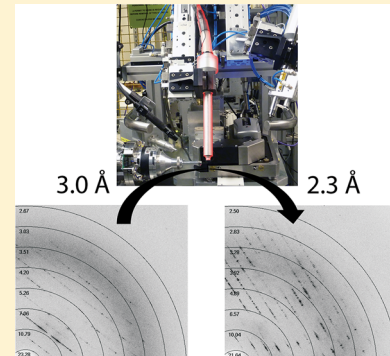
<sup>♯</sup>Department of Biochemistry and Structural Biology, Centre of Molecular Protein Science, Lund University, P. O. Box 124, SE-22100 Lund, Sweden

<sup>▽</sup>Department of Physics, University of Oxford, Keble Road, Oxford OX1 3RH, U.K.

<sup>○</sup>Structural Biology Group, European Synchrotron Radiation Facility, 71 avenue des Martyrs, CS 40220 F-38043 Grenoble, France

### Supporting Information

**ABSTRACT:** Controlled dehydration of macromolecular crystals can lead to significant improvements in crystalline order, which often manifests itself in higher diffraction quality. Devices that can accurately control the humidity surrounding crystals on a beamline have led to this technique being increasingly adopted as experiments become easier and more reproducible. However, these experiments are often carried out by trial and error, and in order to facilitate and streamline them four European synchrotrons have established a collaboration around the HC1b dehydration device. The MAX IV Laboratory, Diamond Light Source, BESSY II, and the EMBL Grenoble Outstation/ESRF have pooled information gathered from user experiments, and on the use of the device, to propose a set of guidelines for these experiments. Here, we present the status and automation of the installations, advice on how best to perform experiments using the device, and an analysis of successful experiments that begins to show some trends in the type of protocols required by some systems. The dehydration methods shown are applicable to any device that allows control of the relative humidity of the air surrounding a macromolecular crystal.



### 1.0. INTRODUCTION

When initial crystals of biological macromolecules become available, they are often too small to be useful or do not exhibit the diffraction properties required for successful structure determination. Therefore, the first task is to improve the quality of their diffraction properties. There are a multitude of methods that exist to do this, from optimization of crystallization conditions and changing the construct that is used for crystallization<sup>1</sup> all the way to working on the obtained crystals themselves by applying postcrystallization treatments.<sup>2,3</sup> Usually, a number of rounds of optimization are required.<sup>3</sup> One of these postcrystallization tools is the dehydration of crystals. This can be performed either by the removal of water in the mother liquor or by controlled reduction of the relative humidity (RH) surrounding the crystal. This technique has been known to alter the properties of crystals since Max Perutz's pioneering

experiments in the 1940s.<sup>4</sup> Since then, many examples have been found, but these occurred often by accident<sup>5–16</sup> rather than design.<sup>17–27</sup> In an effort to characterize and control these effects, several devices have been developed in order to control the humidity surrounding crystals.<sup>28–30</sup> The more recently developed devices have been designed with the goal of being compatible with X-ray sources in order to directly observe the effects of humidity on the diffraction characteristics of the crystal being studied.<sup>31–33</sup> These devices moved the study of crystal dehydration into a new realm as humidity could be controlled precisely while monitoring the effects through diffraction, but they were often difficult to install on rotating anode generators or

**Received:** June 18, 2014

**Revised:** January 12, 2015

**Published:** January 13, 2015

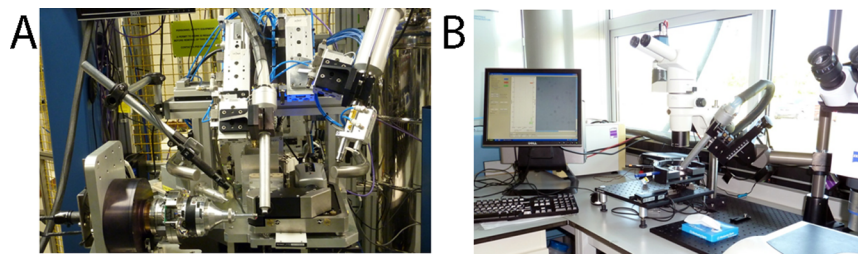


**Figure 1.** The HC1 at Diamond Light Source: (A) Overall view of the installation on beamline I02 showing the pneumatic drive that switches between the HC1 (at the sample position) and cryostream (right); (B) offline setup showing from the left the control computer (running the HC1 software), the sample holder, microscope, and HC1 assembly, and the sample handling microscope.

synchrotron beamlines. The latter limitation stimulated the development of a new device at the EMBL Grenoble Outstation, the HC1b.<sup>24,34</sup> The HC1b produces an air stream with controlled relative humidity using a dispensing nozzle, in the same manner as cryostream devices produce a nitrogen flow at 100 K, and is therefore easy to integrate with most diffractometers. It supplies a stream of humid air at a precisely controlled RH determined by a dew point controller acting on a water saturated air supply. The device is now installed at laboratories and synchrotrons across the world, resulting in many successful experiments; for some recent examples see refs 21 and 35–38. However, the technique still lacks a set of general rules or conditions, meaning that many experiments are performed by trial and error. This led to a collaboration between European Synchrotron sites (EMBL/ESRF, Grenoble, France; Diamond Light Source, U.K.; BESSY II, Germany; and the MAX IV Laboratory, Sweden) to cooperate on the installation of the devices, gather information from experiments, and develop rules and tools for best practices in dehydration experiments (see <http://www.embl.fr/CrystalDehydrationCollaboration>). Here we present the status of the installations at the different sites, the automation of some of the steps required, basic guidelines for experiments, and examples of successful experiments. We also present some analysis that hints at the protocols that should be used for different samples.

## 2.0. MATERIALS, METHODS, AND RESULTS

**2.1. HC1b Dehydration Device.** The HC1b<sup>34</sup> produces an open stream of air at room temperature with the RH adjustable between 45% and 99.7%. The stream is dispensed by a nozzle designed to use the same mounting as the cryostream devices usually installed on X-ray diffractometers. Crystals are placed in the air stream mounted on mesh loops. The HC1b nozzle is connected via a 1.5 m tube to a control unit containing a generator of water saturated air, a condenser, and control electronics. The system monitors the temperature of the condenser to produce an air flow at the desired RH. The controller is connected via a dedicated ethernet link to a Windows or Linux PC with control software that can be operated either locally or remotely. In local operation, the user changes the RH set point, or starts procedures for dehydration in steps or ramps, monitoring the readout of RH on a chart. Automated experiments can be implemented by writing scripts in Python and are triggered from within the HC1b software or from a Python console. In remote mode, the machine is controlled by higher level software—such as a beamline control package—allowing dehydration protocols involving humidity scans, data collection, and data analysis. In this mode, the HC1b software is accessed through a server interface and the GUI is optional as the software can be started as a console application. Servers are

enabled in the HC1b software by selecting one of the supported communication protocols: standard protocols (Web Services, RMI), typical beamline control systems (e.g., Tango, Tine, and Epics), or an EMBL protocol (Exporter) which has client libraries in C, Python, and Java. The HC1b has been commercialized and is available from Arinax ([www.arinax.com](http://www.arinax.com)).

**2.2. Integration of the Device into Beamline Experimental Environments.** **2.2.1. ESRF/EMBL Beamlines.** Two devices are available on all ESRF beamlines.<sup>39–42</sup> The devices have a dedicated GUI allowing the control of functions as well as predication and refinement of RH equilibrium points. However, coupling the device to subsequent data acquisition and analysis is a more complex operation. At the ESRF/EMBL beamlines a workflow tool, DAWN,<sup>43</sup> has been developed that integrates control of the HC1 with humidity gradient design, data collection, and data analysis through the beamline GUI MXCuBE.<sup>44</sup> The workflow allows the user to define a RH gradient based on target RH and equilibration time and couples each step to automatic data collection and analysis using EDNA<sup>45</sup> that will run the programs LABELIT,<sup>46,47</sup> MOSFLM,<sup>48</sup> and BEST<sup>49</sup> and output charts based on the results. By coupling all of these steps, a typical experiment becomes increasingly reproducible and the analysis consistent. The DAWN workflow tool allows separate steps, such as control of devices or Python scripts (called actors), to be connected in order to link data analysis and instrument control. In this case, TANGO control actors communicate with the HC1 and existing EDNA characterization actors were used to build up the experiment workflow. Users interact with this, and other workflows, through a dedicated tab in MXCuBE allowing interaction at specific points, as the information in the tab changes dynamically. Data are stored in the beamline database ISPyB,<sup>50</sup> and an html page is produced in MXCuBE displaying the various image quality indicators and results of indexing against the RH. Once a phase transition has been characterized, protocols can be repeated without data collection to allow the final protocol for optimization to be performed without exposure to X-rays.

On BM14, a nozzle changer (REX, [www.arinax.com](http://www.arinax.com)) that allows for the fast exchange (less than 1 s) between a cryostream and RH controlled streams has been installed. This allows the flash cooling of dehydrated crystals without manual intervention. The REX also facilitates changing between cryogenic and room temperature or dehydration experiments.

**2.2.2. Diamond.** Two devices are currently available for use on all Diamond MX beamlines (I02, I03, I04, I04-1, and I24) as well as in an offline laboratory. Since beamline hardware is not identical, small changes have been made to make the environments compatible. A pneumatic assembly that allows the automatic exchange between cryogenic and HC1 nozzles has been installed on beamlines I02, I03, and I04; the assembly also

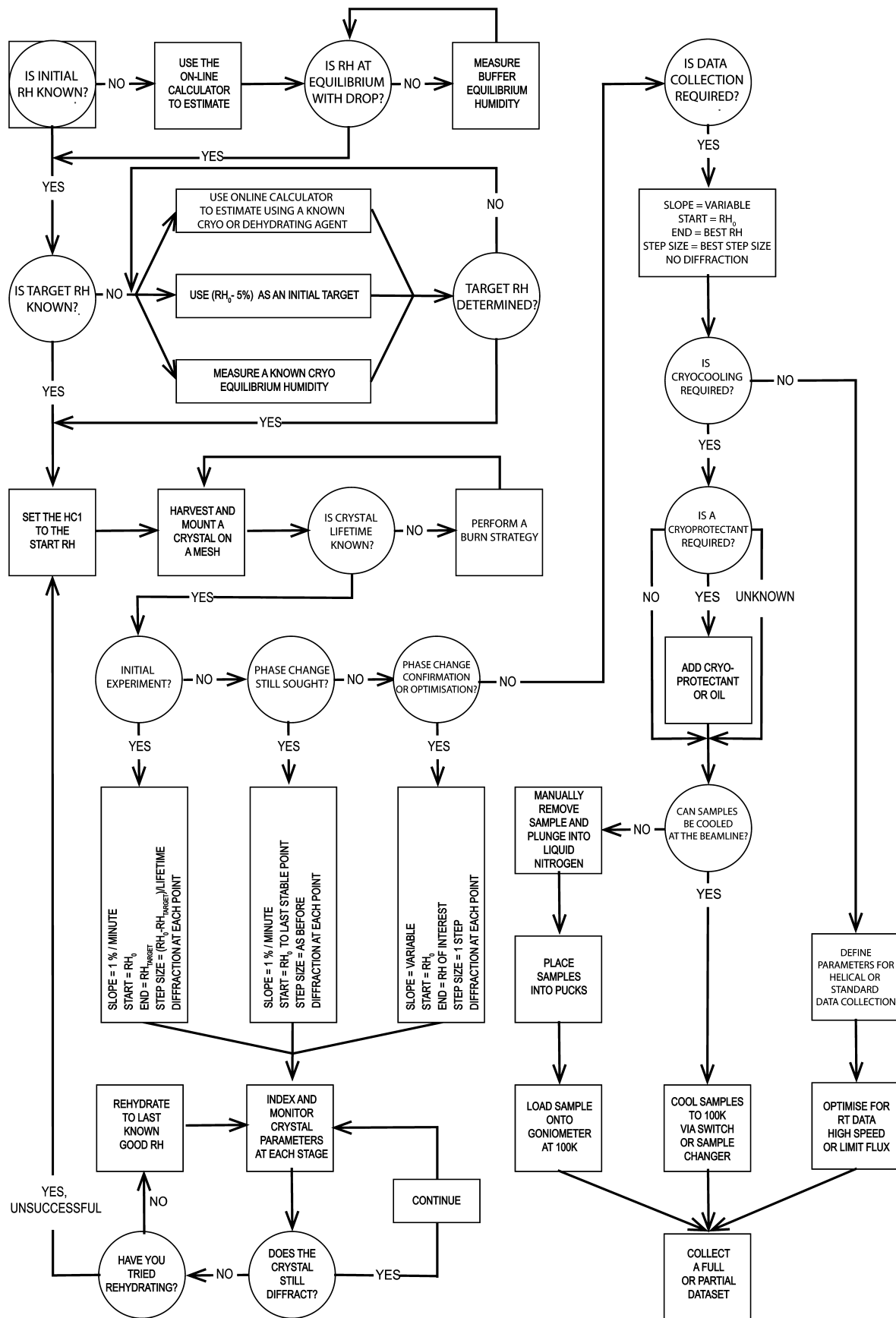


**Figure 2.** Flowchart showing the steps that should be performed in a dehydration experiment.

Table 1. Recommended Steps for an Initial Dehydration Experiment

Experiment Phase	Action and General Considerations
Determine equilibrium RH of mother liquor	The starting point can be determined at <a href="http://go.esrf.eu/RH">http://go.esrf.eu/RH</a> then refined using the HC1 device software. <ul style="list-style-type: none"> <li>Conditions with high concentrations of volatile compounds should be avoided</li> <li>It can be useful to check the RH of known cryoprotectant as a reference</li> </ul>
Mount crystal and assess diffraction quality of crystal before dehydration, test for sensitivity to radiation damage	Crystals should be mounted on mesh loops and excess mother liquor removed. <ul style="list-style-type: none"> <li>Determine diffraction characteristics of crystal (unit cell, diffraction limit)</li> <li>Determine the life time of crystal</li> <li>Determine number of images and exposure time for robust indexing</li> <li>Assess possibility to collect a RT dataset</li> </ul>
Slowly dehydrate crystals while monitoring diffraction quality and unit cell parameters	Dehydrate initially in 0.5 - 2% steps from starting point to 10% below while monitoring changes in crystal parameters. <ul style="list-style-type: none"> <li>Equilibration time varies with crystal size, 1 min for micro crystals/thin plates to 5 mins for large crystals.</li> <li>Radiation damage should be monitored carefully.</li> <li>Dehydration damage may be reversible, radiation damage is not.</li> <li>Follow unit cell parameters and/or intensity as measure of change.</li> <li>Follow relative diffraction limit</li> <li>Dehydrate beyond degradation in quality as improvement often appears after a phase transition.</li> </ul>
Once a phase transition has been induced, determine the optimised protocol	Determine the key steps required to obtain a desired result. <ul style="list-style-type: none"> <li>Rate of change and equilibration time are important factors.</li> <li>Initial changes observed may not enhance resolution but the final protocol can often have dramatic effects.</li> <li>Determine if phase transition is reversible</li> <li>Determine rehydration protocols</li> <li>Analyse the effect of adding cryoprotectant</li> <li>Test many samples</li> </ul>
Cryocool crystals	Crystals can be cooled by plunging into liquid nitrogen manually or using a sample changer or nozzle exchange system. <ul style="list-style-type: none"> <li>Most crystals can be directly cryocooled after conditioning if all mother liquor has been removed.</li> <li>If solvent channels are larger than 40 Å oil or cryoprotectant will need to be added before cooling either before or after dehydration.</li> <li>Several samples and protocols will need to be analyzed</li> <li>This can be tested off-line</li> </ul>

allows samples conditioned using the HC1 to be cryocooled within 2 s (Figure 1A). Installation on I04-1 and I24 requires the intervention of the beamline staff but is normally completed within 10 min. The laboratory setup is equipped with a video microscope and a holder with a capacity of five samples (Figure 1B). These samples are mounted on standard magnetic holders making it simple to condition numerous samples and subsequently cryocool them for X-ray analysis. The offline setup is used in combination with scheduled beamtime to increase efficiency. The laboratory is either used after diffraction experiments, to optimize the conditions found at the beamline, or beforehand, to allow the exploration of broad dehydration space before the refinement of dehydration protocols.

Software control depends on the location of the HC1; the generic HC1 software is used in the laboratory and EPICS IOC at the beamline. In the laboratory, the GUI is used to control the RH as well as predict and refinement of RH equilibrium points. At the beamline, the generic GUI runs in the background controlling the device as an EPICS software IOC and users interact with their experiments using the beamline control software, GDA, which communicates with EPICS. Initially,

simple scripts were used to drive dehydration protocols and collect data, but a perspective has been developed in GDA to make the dehydration experiment as intuitive as possible. The perspective is divided into four areas: crystal imaging and centering, RH plot, RH control, and a data collection input table. Users plan their dehydration protocols in separate stages. Each stage consists of an independent number and type of hydration/dehydration steps that can include waiting times, images of crystals, and/or data collections.

Data analysis is currently performed using the Diamond MX pipeline tools. Diffraction images are analyzed with EDNA<sup>45</sup> and MOSFLM.<sup>48</sup> Indexing and strategies are automatically calculated and data are stored in the beamline database ISPyB, and an html page summarizing results is displayed for the users. In the future, it is planned to implement tools similar to the ESRF/EMBL workflows coupled to feedback in GDA and to be able to receive user input for the difficult to index projects.

**2.2.3. Helmholtz-Zentrum Berlin (BESSY II).** At the HZB, the HC1 is installed on the fixed-wavelength beamline BL14.3.<sup>51</sup> This beamline is equipped with a MAR-dtb goniometer and a MX225 CCD detector. The beamline can be easily switched

**Table 2. Observed RH Equilibrium Points for a Series of PEG Molecular Weights and Cryoprotectants at Different Concentrations**

concn (% (w/w))	RH equilibrium point (%)							
	PEG10000	PEG6000	PEG4000	PEG1500	PEG400	PEG200	glycerol	EG
10	99.9	99.9	99.9	99.9	99.9	99.9	99.5	98.5
20	99.9	99.9	99.9	99.9	99.9	99.5	96.5	94.0
30	99.9	99.9	99.9	99.9	98.8	97.3	92.0	89.5
40	99.3	99.9	99.2	98.3	96.3	94.9	88.5	85.0
50		99.25	97.6	95.8	93.5	90.2	84.0	79.0

between HC1 operation and operation using a cryostream within 10 min. For sample viewing, a high resolution video microscope has been installed which is interfaced to the HC1 operating software. Currently, there is no direct link between beamline operation and HC1 operation. The installation of MXCuBE<sup>44</sup> on this beamline is planned, thus alleviating the need to switch between two different computer programs during an HC1 experiment.

**2.2.4. MAX IV Laboratory.** The HC1 at the MAX IV Laboratory is installed at the multiwavelength beamline I911-3 at the MAX-II storage ring.<sup>52</sup> This beamline is equipped with a MD2 (ARINAX, Moirans, France) and a MX225 CCD detector (MAR research, Norderstedt, Germany). A CATS automatic sample changer is also installed and is used to harvest crystals conditioned by the HC1. Under normal operation of the beamline, a cryostream is used to maintain the samples in a stream of cold nitrogen. This can be replaced by the HC1 within 10 min. Because the MD2 provides an on-axis microscope view of the sample, this viewing system is interfaced with the HC1 operating software. In the present setup the HC1 software is used standalone, while data collection is performed with MXCuBE. The full integration of HC1 control within the MXCuBE environment is foreseen.

**2.3. Experiment Setup, Design, and Protocols.** Much has been learned from the use of the device at the various sites, and this has been distilled into a general protocol that should be followed for initial dehydration experiments (Figure 2 and Table 1). No two systems require the same protocol, but for initial experiments a standard workflow can be employed. Figure 2 shows the detailed steps in the process, and the main actions are described here and in Table 1. First, the RH starting point must be found by determining the RH in equilibrium with the mother liquor (see section 2.3.1 for further details). Second, the crystal is subjected to slow dehydration while monitoring diffraction characteristics. This step is performed using RH steps between 0.5 and 2% with an initial target RH of 10% below the equilibrium point. The equilibration time required correlates strongly with crystal size and microcrystals or thin plates (<20 μm in their largest dimensions) require ca. 1 min for equilibration, whereas large crystals (>200–500 μm in their largest dimensions) require ca. 5 min. This step allows phase transition points to be determined. Phase transitions are characterized by significant changes in unit cell dimensions, diffraction intensity, or space group. If no phase transitions are found, diffraction is lost completely over a narrow RH range as the lattice breaks down, but diffraction can often be recovered by returning the RH to the starting point. This is in contrast to phase transitions, where degradation in diffraction quality is often observed as the lattice rearranges, but diffraction is not completely lost. This is demonstrated in a movie (see the Supporting Information) showing the loss of diffraction from crystals of the TANK binding kinase.<sup>53</sup> For comparison, a phase transition observed between a RH of 99.0 and 97.0% for crystals of photosystem II, as

previously described,<sup>24</sup> is also shown. The movie shows diffraction images from the starting point of 99% to 97.5% RH where diffraction is completely lost, the final image shows the recovery of diffraction after the RH is returned to 99%. In these cases, dehydration will not usually be successful with the system being studied and the experiments can be terminated. However, if phase transitions are observed, a large variety of protocols may need to be employed to attain an increase in diffraction quality within the RH range determined. Determination of the protocol involves the variation of all parameters, including speed of dehydration, equilibration time, rehydration cycles, and the number of steps. Once a successful protocol has been defined, the final step is to cryocool the crystals. It has been found that crystals can often be directly cryocooled without the addition of cryoprotectants if all mother liquor has been removed.<sup>54</sup> However, if the crystals contain large solvent channels, oil or cryoprotectant solutions will need to be added before cooling. Table 1 and Figure 2 contain more specific advice for each step.

**2.3.1. Prediction of the Mother Liquor Equilibrium Relative Humidity for Solutions of PEG Using Raoult's Law and the Flory–Huggins Model for the Entropy of Mixing of Polymers.** The first step in a dehydration experiment is to determine the RH in equilibrium with the mother liquor of the crystal being studied. If the value to which the crystal is exposed is too high, it will dissolve, and if too low, rapid and irreversible changes in the crystal may be induced. Until recently, the equilibrium RH has been determined experimentally by placing a drop of the mother liquor in a loop and monitoring the size of the drop using image processing software. This stage of the experiment can be quite time-consuming as an initial starting point is often unknown. In order to simplify this process, we measured the equilibrium RH for a range of concentrations of the most commonly used precipitants (salts and polymers such as poly(ethylene glycol) (PEG)). The data provide a starting point for most dehydration experiments, and Raoult's law, for the equilibrium vapor pressure of water above a solution, can be used to understand the observations and make predictions for precipitant concentrations commonly in use.<sup>55</sup> For salts and small molecules a reasonably linear relationship between mole fraction and RH equilibrium point was found. For PEGs, increasing the molecular weight (for a given weight/weight concentration) increased the RH in equilibrium with the solution and a steep increase in RH equilibrium point with decreasing PEG concentration was observed. Measurements were also made of typical buffer solutions (100 mM) and detergents (1% (w/v)), and these were found to have an RH equilibrium point of close to 100%. Therefore, it can be concluded that only the main precipitant affects the RH equilibrium point. In order to illustrate the variation of RH equilibrium points with common precipitant concentration series, the data collected in the previous study<sup>55</sup> are presented in Tables 2 and 3.

Using Raoult's law,<sup>56</sup> the equilibrium relative humidity can be predicted for many of the precipitants used in macromolecular

**Table 3. Observed RH Equilibrium Points for a Series of Salts at Different Concentrations**

concn (M)	RH equilibrium point (%)			
	NaCl	sodium acetate	sodium malonate	ammonium sulfate
0.5	99.8	99.9	99.9	99.9
1	98.9	98.9	99.25	99.1
1.5	97.2	97.1	97.0	97.7
2	95.3	94.8	95.2	95.9
2.5	94.2	93.2	92.5	94.3
3.0	92.8	91.2	89.9	92.8

crystallogenesis. Since performing these measurements, we have extended the model to account for large polymers. Raoult's law starts to break down for polymer solutions over a molecular weight of 1000 Da, but this can be corrected using the Flory–Huggins model<sup>57–59</sup> for the entropy of mixing of polymers:

$$RH = \frac{1}{1 + \frac{18x}{(1-x)m}} e^{\{(1-m/n)/(1+\frac{(1-x)m}{18x})\}} \quad (1)$$

where RH is the relative humidity,  $x$  is the mass fraction of solute,  $n$  is the molecular weight of the polymer, and  $m$  is a parameter for a polymer such that the ratio  $n/m$  is the number of segments of polymer, each of which takes up one space in the disordered lattice. We have found that a value of  $m = 38$  Da gives the best fit to experimental data<sup>55,60,61</sup> rather than the actual value of 44 Da for PEG. Thus,  $m$  is approximately the molecular weight of the monomer, when each of the segments is a monomer. For  $n \gg m$  the dependence on  $n$  diminishes as a function of the mass fraction  $x$ , so the relative humidity curve has a nearly universal shape for polymers of molecular mass above ca. 1000 Da. Therefore, the RH equilibrium points for all PEGs of >1000 Da will be roughly equal. As previously observed, there is a discrepancy between measured values and those predicted by theory<sup>55</sup> where measured values are approximately 1% higher. This is accounted for by the difficulties in accurately maintaining relative humidities above 96% and differences in the measurement environment. Nonetheless, the predicted values provide an excellent starting point for the determination of equilibrium RH points. An online calculator is available, based on the equations derived from this work, to allow users to predict the RH starting points in advance of experiments (<http://go.esrf.eu/RH>). In addition, a refinement strategy has been incorporated into the HC1 control software. Images of the drop are processed, and the drop size is estimated and plotted every second. The device then automatically regulates the RH as a function of the measured drop size until the drop is stable. This allows the RH to be set to a predicted value; a drop of mother liquor is then placed on a loop and its size monitored; the process takes less than 5 min.

**2.3.2. Examples of Successful Protocols. 2.3.2.1. Ambient Temperature Data Collection.** The emergence of pixel array detectors that allow continuous readout at high speed<sup>62</sup> has led to a renaissance of room temperature (RT) data collection with the intriguing possibility of "out running" the increased radiation damage.<sup>63–65</sup> It is also often advantageous to characterize diffraction quality from crystals before cryocooling in order to assess the effects of cryoprotectant solutions. The ease of mounting samples with the HC1 makes it the ideal support for RT collections as it obviates the need for a capillary and subsequent alteration of the diffractometer. Additionally, as all equipment usually available on a beamline is compatible with these experiments, this allows the use of miniKappa goniometers,<sup>66</sup> microspectrophotometers,<sup>67,68</sup> and helical data

collection to constantly expose fresh crystal volumes to reduce radiation damage.<sup>24,40</sup> In addition, the background is lower than when capillary devices are used. Crystals are mounted at the equilibrium RH for the mother liquor, in the same manner as for a dehydration experiment, and the liquid can either be wicked away (by touching tissue paper to the reverse of a mesh loop) or left in order to increase the stability of the crystals.

While collecting at ambient temperature presents many difficulties compared to cryogenic data collection, it can also offer many advantages. This was the case for a protein–protein complex involved in cofactor biogenesis (A. Pearson, personal communication). Crystals had been obtained, but cryoprotection was problematic and regions of the complex were disordered in the final maps. Therefore, dehydration was attempted as a way to increase the order in the crystals. Crystals were obtained in midrange PEG solutions and were mounted at a RH of 99.5% using the HC1 on the ESRF beamline ID29. Initial assessment of images collected at room temperature demonstrated greater order with respect to cryocooled crystals without further treatment, and it was decided to collect a data set at this RH. A strategy was calculated to minimize radiation damage collecting 116° with 0.05° oscillations at 0.5% transmission of the beam (full flux,  $2.24 \times 10^{13}$  photons/s) with a PILATUS 6 M detector (Dectris Ltd., Baden, Switzerland) operating at a frame rate of 25 Hz. This led to the collection of a data set to 1.6 Å of excellent quality (Table 4). When the density maps were inspected, it was revealed that the complete complex was visible.

**Table 4. Data Collection and Processing Details for a Sample Ambient Temperature Data Set**

temp (K)	293
wavelength (Å)	0.976
flux (0.5% transmission, photons/s)	$1.12 \times 10^{10}$
oscillation (deg)	0.05
exposure time/image (s)	0.037
total exposure time (s)	85.8
dose (MGy)	0.04
space group	I4
unit cell dimens (Å): $a, b, c$	86.3, 86.3, 80.9
$\alpha, \beta, \gamma$ (deg)	90.0, 90.0, 90.0
resoln range <sup>a</sup> (Å)	43.2–1.62 (1.68–1.62)
no. of unique reflecs <sup>a</sup>	36939 (8929)
multiplicity <sup>a</sup>	4.2 (2.8)
completeness <sup>a</sup> (%)	97.7 (84.8)
$R_{\text{merge}}^{\text{a},\text{b}}$	0.06 (0.51)
$\langle I/\sigma(I) \rangle^{\text{a}}$	12.3 (1.7)
Wilson B factor (Å <sup>2</sup> )	17

<sup>a</sup>Statistics for the highest resolution bin are shown in parentheses.

<sup>b</sup> $R_{\text{merge}} = \sum_{h} \sum_i |I(h) - \bar{I}(h)| / \sum_{h} \sum_i I(h)_i$ , where  $I(h)$  is the mean weighted intensity after rejection of outliers.

**2.3.2.2. Space Group Change and Resolution Improvement.** Monoclinic crystals of a viral protein from cytomegalovirus (CMV) were subjected to a controlled dehydration experiment on HZB-MX BL14.3. The initial RH was determined to be 98% by observing the size of a drop of reservoir solution. A crystal was mounted on a micromesh in an air stream of 98% RH, and excess mother liquor was removed using a paper wick. The initial diffraction extended visibly to approximately 3.0 Å. The RH was then reduced in 2% steps with a 4 min equilibration between steps. At an RH of approximately 88%, the diffraction pattern began to change, and after a further reduction of the RH

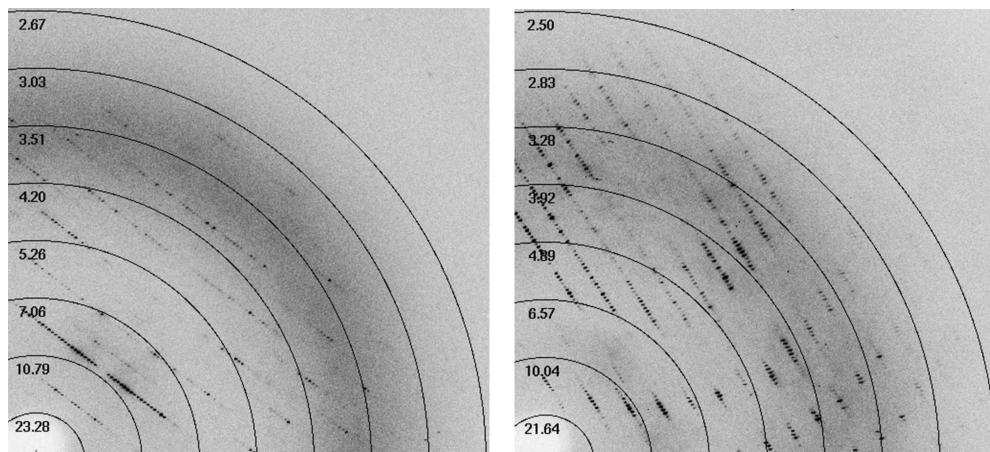


**Figure 3.** Diffraction images of two crystals of a CMV viral protein. For the left panel, the crystal was flash-cooled to 100 K from a RH of 98%. Diffraction spots are visible to about 3 Å resolution, and the corresponding space group is  $P2_1$ . For the right panel, the crystal was flash-cooled to 100 K after dehydration to a RH of 86%. Here, visible reflections extend to beyond 2.5 Å resolution. The corresponding space group is  $P4_3$ .

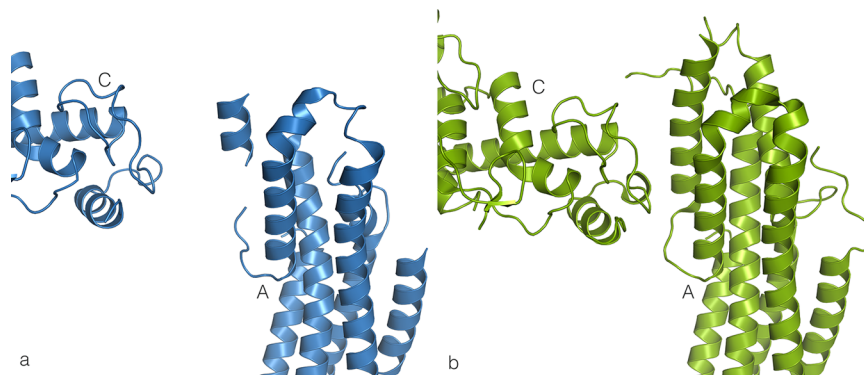


**Figure 4.** Crystallographic contacts between chains A and C of the “native” (panel a in blue at a RH of 96%) and dehydrated (panel b in green at a RH of 86%) forms of glypcan1 crystals. (Adapted with permission from ref 72 (Awad et al.). Copyright 2013 International Union of Crystallography.)

to 86%, the visible diffraction extended to approximately 2.4 Å (Figure 3). Decreasing the RH further resulted in a decrease in diffraction quality. The crystal was then cryocooled by immersing it in liquid nitrogen, and a complete data set was collected at 100 K. The diffraction limit of this data set was 2.3 Å. The reduction of the RH from 98% to 86% led to a change in space group from monoclinic  $P2_1$  to tetragonal  $P4_3$  and a reduction of the unit cell volume by more than 10%. Further details are published elsewhere.<sup>69</sup>

**2.3.2.3. Anisotropy Reduction and Improved Model.** Human glypcan 1 core protein crystals<sup>70</sup> are formed as delicate fragile plates with a solvent content of 56%. After cryoprotection, the crystals display poor isomorphism with variations in the cell dimensions, in particular the *c* axis which varies between 147 and 155 Å. The structure of the protein was determined to 2.55 Å resolution, but the crystals diffracted anisotropically with a Wilson B factor twice as large in the *c*\* direction than in either the *a*\* or *b*\* directions. The resolution in the *c*\* direction was also limited to 2.9 Å. In addition, part of the structure of the protein was disordered and could not be traced in electron density maps. Because refinement using ellipsoidally truncated data produced by the UCLA MBI diffraction anisotropy server<sup>71</sup> did not give better results than using 2.55 Å anisotropic data, the latter was used for the structure determination. A systemic study using the HC1 at I911-3<sup>72</sup> was performed to investigate whether controlled crystal dehydration could decrease the anisotropy in the diffraction behavior of the glypcan 1 core protein crystals.

Therefore, a number of parameters (dehydration rate, final relative humidity, and total incubation time) were tested for their importance in obtaining an optimal protocol for dehydration leading to a more isotropic diffracting system. After initial experiments using the standard protocol, it appeared that for this system the total incubation time is the most important factor, while the dehydration rate and final humidity seem to be less important. A slight improvement in resolution (from 2.55 to 2.46 Å) was obtained for a crystal where the humidity was decreased to 86% (from 96%) in 0.1% steps of 30 s; the crystal was subsequently flash-cooled using the CATS robot. The total dehydration time was 61 min. Although the overall resolution did not increase dramatically, the anisotropic behavior was decreased significantly and the overall quality of the data was increased accordingly. This was most prominent in electron density maps of improved quality which made it possible to place an additional 56 amino acid residues and 124 water molecules in the model (Figure 4). The crystal packing was affected by the controlled dehydration and a large increase in contacts between the symmetry related molecules could be observed.

**2.3.2.4. DNA Conformation Change.** Tetragonal ( $P4_32_12$ ) crystals of a duplex DNA oligonucleotide<sup>73</sup> were subjected to a controlled dehydration experiment on beamline I02 at Diamond. Initial tests started at a RH of 97% ( $a = b = 42.9 \text{ \AA}$ ,  $c = 39.5 \text{ \AA}$ ) and ended at a RH of 74%, recording diffraction images at every 1% step. These crystals exhibited a phase transition at a RH of 84% that subsequently yielded a new stable unit cell at a RH of 74% ( $a$

$a = b = 44.3 \text{ \AA}$ ,  $c = 27.5 \text{ \AA}$ ). It was also possible to rehydrate these crystals by reverting to a RH of 99%, returning them to their original unit cell dimensions ( $a = b = 42.9 \text{ \AA}$ ,  $c = 38.4 \text{ \AA}$ ). It was possible to collect seven full data sets at room temperature from the same sample, and the structures have been successfully refined (Figure 5). The structures show a partial B-DNA to A-DNA conformation change and the presence of a 51° kink when dehydrated. Further details have been published elsewhere.<sup>74</sup>

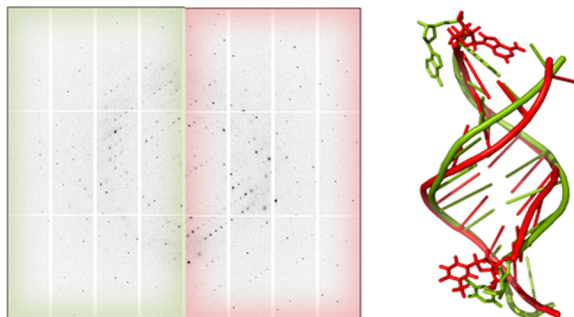


**Figure 5.** DNA dehydration. Diffraction patterns at RH of 97% (left, green) and 74% (red) with diffraction limits of 1.5 and 1.18 Å, respectively. The corresponding refined models are shown colored similarly.

**2.3.2.5. Membrane Protein Crystal Resolution Improvement.** Crystals of a homologue of the bile acid sodium symporter ASBT<sup>35</sup> were subjected to controlled dehydration using the protocol described here. After initial experiments, changes in unit cell parameters were observed after long dehydration runs but with no improvement in diffraction limit. An extreme dehydration protocol was then performed, decreasing from an initial RH of 98% to 45% in a single step. This large hydration difference led to an improved diffraction limit at room temperature from around 10 Å to approximately 4 Å and yielded a greatly increased resolution limit upon cryocooling. The final protocol, carried out offline, involved the immediate transfer of samples into the air stream at a RH of 45% followed by a 5 min equilibration time prior to cryocooling. This procedure led to the collection of a 1.8 Å data set.<sup>35</sup> Low hydration protocols could be a more common requirement of membrane proteins rather than soluble ones. Type II membrane protein crystals have very few lattice contacts between symmetry related molecules, and large areas of loose detergent contacts could allow new contacts between soluble moieties to be formed under these extreme conditions.

### 3.0. DISCUSSION

While the general steps for a humidity control experiment are now well-defined, little is known about the types of system that will respond well to dehydration. In order to gain insight into these processes the results in the literature from 79 systems where dehydration has had a beneficial effect have been analyzed (see Supporting Information for a list of references and the data extracted). This includes many cases where a humidity control device was not used. While the results of this analysis do not provide an answer as to which systems will be amenable to dehydration, they are nevertheless informative.

The main characteristics analyzed were the crystal system, the molecular weight of the entity crystallized, the change in RH required for the phase transition, and the starting and final resolution limits. Where RH changes were not given, they were

estimated from the content of the mother liquor and dehydrating solution. The first parameter investigated was the crystal system. It has been suggested that lower symmetry space groups could be more amenable to dehydration due to fewer constraints on the unit cell parameters.<sup>34</sup> Plotting the crystal system of the examples against the RH change required shows that the distribution of symmetry exactly matches that of nonredundant structures in the Protein Data Bank (PDB)<sup>75,76</sup> and that there is no obvious correlation between symmetry and the size of RH decrease required (Figure 6A). There also appears to be a much higher

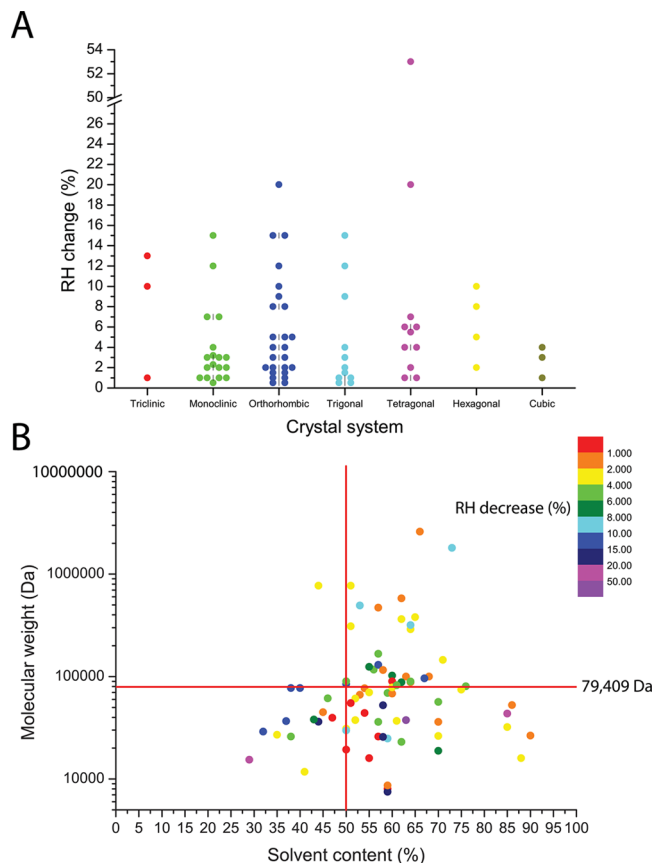


**Figure 6.** (A) Analysis of all published successful dehydration experiments. A distribution of the point groups against the change in RH required. (B) Distribution of molecular weight against final solvent content. Positions are colored according to RH decrease, and red lines show the average value for molecular weight of the entity crystallized and the peak value for solvent content in the PDB.

proportion of systems where a small change (<5%) is required. However, the change in RH is often underestimated where dehydration was performed by soaking in different solutions, as any dehydration due to evaporation will not be accounted for. Symmetry does not appear to be a factor, but molecular weight and solvent content are also factors important in crystal packing. Plotting these measures against each other and coloring by RH decrease shows some interesting trends (Figure 6B). Of the systems amenable to dehydration, 75% have a solvent content over 50% (the most frequent value in a distribution of PDB entries), and there are also a significant number of large complexes. This may be due to a bias introduced by the large number of challenging projects that tend to be prioritized for potential improvements in diffraction quality. A clear trend is that crystals of low molecular weight macromolecules require larger

changes in RH, possibly to overcome the greater stability arising from more crystal contacts and that large complexes typically require much smaller changes (Figure 6B). While many beneficial changes can be induced by dehydration (symmetry increase, reduction in asymmetric unit, reduction in anisotropy, and increased homogeneity<sup>77</sup>), the ultimate aim is usually to increase the resolution limit. Comparing initial and final resolution limits (when available) shows interesting features (Figure 7). It is clear that the resolutions obtained before

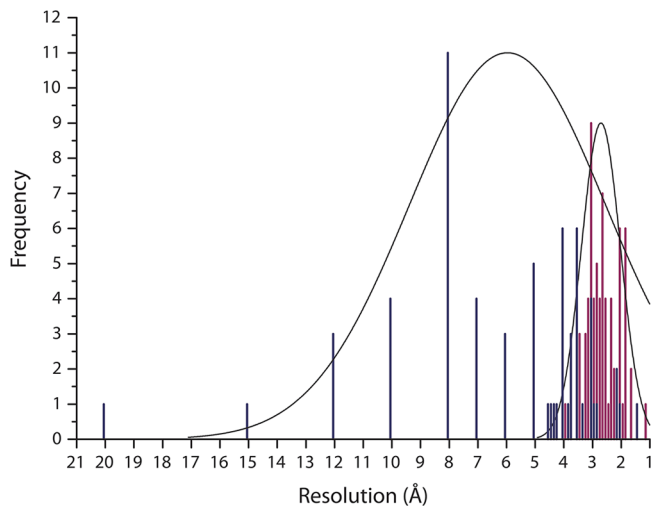


**Figure 7.** Histogram of initial resolution (blue) and final obtained resolution (purple) from successful dehydration experiments. Normal distribution curves are shown with peaks at 6 (before) and 2.8 Å (after).

dehydration are lower and more widely spread than after conditioning when they cluster around 2.8 Å. The most frequent starting resolutions are around 8 and 4 Å with the final level around 3 Å. This demonstrates that when dehydration is successful, significant increases in resolution are obtained. What is clear from this analysis is that dehydration can be successful regardless of symmetry, molecular weight or solvent content and should always be attempted.

#### 4.0. CONCLUSION

The device is now widely available and experiments have become increasingly routine to perform. However, further developments will increase the use and importance of the method. A technique that has not yet been exploited is the use of cross-crystal averaging between different hydration states. This technique can be used to improve density maps and also calculate phases for one crystal form from the phase information of another.<sup>78–80</sup> Low resolution phases already obtained could then easily be extended to a higher resolution data set from a dehydrated crystal form, without the need to interpret low resolution maps, a notoriously difficult process. Further automation and the introduction of new experiments could still improve the method. For example, it would be beneficial to determine a crystal's sensitivity to radiation damage at room temperature<sup>81</sup> before starting a dehydration protocol in order to determine how many steps can be made before the crystal will need to be changed. Recent developments in automatic crystal mounting<sup>82–84</sup> could move dehydration experiments into a new phase. If crystals obtained from high throughput screening could be automatically tested for their diffraction properties and then screened for susceptibility to dehydration, more systems could be identified

and improvements pursued using the technique. Coupled to automatic harvesters this could also allow serial crystallography to be performed on small crystals that could be harvested in batches.<sup>85</sup> Despite the many potential benefits of dehydration, the technique has still only been applied to a very small number of samples. Further automation will be required to open the technique to a larger number of samples which may provide further insight into the mechanisms at work.

#### ■ ASSOCIATED CONTENT

##### ● Supporting Information

Table containing all data and primary references for the analysis of successful dehydration experiments and video demonstrating the reversibility of loss of diffraction from dehydration. This material is available free of charge via the Internet at <http://pubs.acs.org>.

#### ■ AUTHOR INFORMATION

##### Corresponding Authors

\*(M.W.B.) E-mail: mbowler@embl.fr. Tel.: 0033 476 20 76 37. Fax: 0033 476 20 71 99.

\*(F.C.) E-mail: cipriani@embl.fr. Tel.: 0033 476 20 75 99. Fax: 0033 476 20 71 99.

##### Present Address

◆ SSRL, SLAC, 2575 Sand Hill Road MS 99, Menlo Park, CA 95124, USA.

##### Notes

The authors declare the following competing financial interest(s): As co-inventors of the HC1, F.C., J.S.-W., and A.G. receive an EMBL invention reward following sales of the HC1 by Arinax.

#### ■ ACKNOWLEDGMENTS

We thank Julien Huet (Arinax, France) and Franck Felisaz (EMBL, Grenoble Outstation) for initial developments for the HC1. We are grateful to Stefan Klingl and Yves Muller (University of Erlangen), Arwen Pearson (University of Leeds), Derek Logan and Wael Awad (University of Lund), and James Hall (University of Reading) for sharing results from HC1 experiments before publication. We thank the Partnership for Structural Biology (PSB), Grenoble, and the Joint Berlin MX-Laboratory for integrated structural biology environments.

#### ■ REFERENCES

- (1) Longenecker, K. L.; Garrard, S. M.; Sheffield, P. J.; Derewenda, Z. S. Protein crystallization by rational mutagenesis of surface residues: Lys to Ala mutations promote crystallization of RhoGDI. *Acta Crystallogr., Sect. D: Biol. Crystallogr.* **2001**, *57* (5), 679–688.
- (2) Heras, B.; Martin, J. L. Post-crystallization treatments for improving diffraction quality of protein crystals. *Acta Crystallogr., Sect. D: Biol. Crystallogr.* **2005**, *61*, 1173–1180.
- (3) Newman, J. A review of techniques for maximizing diffraction from a protein crystal in stilla. *Acta Crystallogr., Sect. D: Biol. Crystallogr.* **2006**, *62* (Pt 1), 27–31.
- (4) Perutz, M. F. The composition and swelling properties of haemoglobin crystals. *Trans. Faraday Soc.* **1946**, *B42*, 187–195.
- (5) Abergel, C. Spectacular improvement of X-ray diffraction through fast desiccation of protein crystals. *Acta Crystallogr., Sect. D: Biol. Crystallogr.* **2004**, *60* (Pt 8), 1413–1416.
- (6) Adachi, H.; Umena, Y.; Enami, I.; Henmi, T.; Kamiya, N.; Shen, J. R. Towards structural elucidation of eukaryotic photosystem II: Purification, crystallization and preliminary X-ray diffraction analysis of photosystem II from a red alga. *Biochim. Biophys. Acta, Bioenerg.* **2009**, *1787* (2), 121–128.

- (7) Cramer, P.; Bushnell, D. A.; Fu, J. H.; Gnatt, A. L.; Maier-Davis, B.; Thompson, N. E.; Burgess, R. R.; Edwards, A. M.; David, P. R.; Kornberg, R. D. Architecture of RNA polymerase II and implications for the transcription mechanism. *Science* **2000**, *288* (5466), 640–649.
- (8) Esnouf, R. M.; Ren, J.; Garman, E. F.; Somers, D. O.; Ross, C. K.; Jones, E. Y.; Stammers, D. K.; Stuart, D. I. Continuous and discontinuous changes in the unit cell of HIV-1 reverse transcriptase crystals on dehydration. *Acta Crystallogr., Sect. D: Biol. Crystallogr.* **1998**, *54* (Pt 5), 938–53.
- (9) Fratini, A. V.; Kopka, M. L.; Drew, H. R.; Dickerson, R. E. Reversible Bending and Helix Geometry in a B-DNA Dodecamer—CGCGAATTBRCGCG. *J. Biol. Chem.* **1982**, *257* (24), 4686–4707.
- (10) Gupta, V.; Gupta, R. K.; Khare, G.; Salunke, D. M.; Surolia, A.; Tyagi, A. K. Structural Ordering of Disordered Ligand-Binding Loops of Biotin Protein Ligase into Active Conformations as a Consequence of Dehydration. *PLoS One* **2010**, *5* (2), No. e9222.
- (11) Heras, B.; Edeling, M. A.; Byriel, K. A.; Jones, A.; Raina, S.; Martin, J. L. Dehydration converts DsbG crystal diffraction from low to high resolution. *Structure* **2003**, *11* (2), 139–145.
- (12) Kuo, A.; Bowler, M. W.; Zimmer, J.; Antcliff, J. F.; Doyle, D. A. Increasing the diffraction limit and internal order of a membrane protein crystal by dehydration. *J. Struct. Biol.* **2003**, *141* (2), 97–102.
- (13) Nakamura, A.; Wada, C.; Miki, K. Expression and purification of F-plasmid RepE and preliminary X-ray crystallographic study of its complex with operator DNA. *Acta Crystallogr., Sect. F: Struct. Biol. Cryst. Commun.* **2007**, *63*, 346–349.
- (14) Sam, M. D.; Abbani, M. A.; Cascio, D.; Johnson, R. C.; Clubb, R. T. Crystallization, dehydration and preliminary X-ray analysis of excisionase (Xis) proteins cooperatively bound to DNA. *Acta Crystallogr., Sect. F: Struct. Biol. Cryst. Commun.* **2006**, *62*, 825–828.
- (15) Vijayalakshmi, L.; Krishna, R.; Sankaranarayanan, R.; Vijayan, M. An asymmetric dimer of beta-lactoglobulin in a low humidity crystal form—Structural changes that accompany partial dehydration and protein action. *Proteins: Struct., Funct., Bioinf.* **2008**, *71* (1), 241–249.
- (16) Yap, T. L.; Chen, Y. L.; Xu, T.; Wen, D. Y.; Vasudevan, S. G.; Lescar, J. A multi-step strategy to obtain crystals of the dengue virus RNA-dependent RNA polymerase that diffract to high resolution. *Acta Crystallogr., Sect. F: Struct. Biol. Cryst. Commun.* **2007**, *63*, 78–83.
- (17) Bowler, M. W.; Montgomery, M. G.; Leslie, A. G.; Walker, J. E. Reproducible improvements in order and diffraction limit of crystals of bovine mitochondrial F<sub>1</sub>-ATPase by controlled dehydration. *Acta Crystallogr., Sect. D: Biol. Crystallogr.* **2006**, *62*, 991–995.
- (18) Dobbek, H.; Gremer, L.; Meyer, O.; Huber, R. Crystal structure and mechanism of CO dehydrogenase, a molybdo iron-sulfur flavoprotein containing S-selanyl cysteine. *Proc. Natl. Acad. Sci. U. S. A.* **1999**, *96* (16), 8884–8889.
- (19) Engel, M.; Hoffmann, T.; Wagner, L.; Wermann, M.; Heiser, U.; Kiefersauer, R.; Huber, R.; Bode, W.; Demuth, H. U.; Brandstetter, H. The crystal structure of dipeptidyl peptidase IV(CD26) reveals its functional regulation and enzymatic mechanism. *Proc. Natl. Acad. Sci. U. S. A.* **2003**, *100* (9), 5063–5068.
- (20) Henrich, S.; Cameron, A.; Bourenkov, G. P.; Kiefersauer, R.; Huber, R.; Lindberg, I.; Bode, W.; Than, M. E. The crystal structure of the proprotein processing proteinase furin explains its stringent specificity. *Nat. Struct. Biol.* **2003**, *10* (7), 520–526.
- (21) Kadlec, J.; Hallacli, E.; Lipp, M.; Holz, H.; Sanchez-Weatherby, J.; Cusack, S.; Akhtar, A. The molecular basis for the recruitment of MOF and MSL3 into the dosage compensation complex by MSL1. *Nat. Struct. Mol. Biol.* **2011**, *18*, 142–149.
- (22) Koch, M.; Breithaupt, C.; Kiefersauer, R.; Freigang, J.; Huber, R.; Messerschmidt, A. Crystal structure of protoporphyrinogen IX oxidase: A key enzyme in haem and chlorophyll biosynthesis. *EMBO J.* **2004**, *23* (8), 1720–1728.
- (23) Kyrieleis, O. J. P.; Goettig, P.; Kiefersauer, R.; Huber, R.; Brandstetter, H. Crystal structures of the tricorn interacting factor F3 from Thermoplasma acidophilum, a zinc aminopeptidase in three different conformations. *J. Mol. Biol.* **2005**, *349* (4), 787–800.
- (24) Russi, S.; Juers, D. H.; Sanchez-Weatherby, J.; Pellegrini, E.; Mossou, E.; Forsyth, V. T.; Huet, J.; Gobbo, A.; Felisaz, F.; Moya, R.; McSweeney, S. M.; Cusack, S.; Cipriani, F.; Bowler, M. W. Inducing phase changes in crystals of macromolecules: Status and perspectives for controlled crystal dehydration. *J. Struct. Biol.* **2011**, *175* (2), 236–243.
- (25) Zerrad, L.; Merli, A.; Schroder, G. F.; Varga, A.; Graczek, E.; Pernot, P.; Round, A.; Vas, M.; Bowler, M. W. A spring-loaded release mechanism regulates domain movement and catalysis in phosphoglycerate kinase. *J. Biol. Chem.* **2011**, *286* (16), 14040–14048.
- (26) Makde, R. D.; Tan, S. Strategies for crystallizing a chromatin protein in complex with the nucleosome core particle. *Anal. Biochem.* **2013**, *442* (2), 138–145.
- (27) Dobrianov, I.; Kriminski, S.; Taylor, C. L.; Lemay, S. G.; Kimmer, C.; Kisilev, A.; Finkelstein, K. D.; Thorne, R. E. Dynamic response of tetragonal lysozyme crystals to changes in relative humidity: implications for post-growth crystal treatments. *Acta Crystallogr., Sect. D: Biol. Crystallogr.* **2001**, *57* (Pt 1), 61–68.
- (28) Einstein, J. R. Humidity Control Device for Buerger Precession Camera. *J. Sci. Instrum.* **1961**, *38* (11), No. 449.
- (29) Huxley, H. E.; Kendrew, J. C. Discontinuous Lattice Changes in Haemoglobin Crystals. *Acta Crystallogr.* **1953**, *6* (1), 76–80.
- (30) Pickford, M. G.; Garman, E. F.; Jones, E. Y.; Stuart, D. I. A design of crystal mounting cell that allows the controlled variation of humidity at the protein crystal during X-ray diffraction. *J. Appl. Crystallogr.* **1993**, *26*, 465–466.
- (31) Kiefersauer, R.; Stetefeld, J.; GomisRuth, F. X.; Romao, M. J.; Lottspeich, F.; Huber, R. Protein-crystal density by volume measurement and amino-acid analysis. *J. Appl. Crystallogr.* **1996**, *29*, 311–317.
- (32) Kiefersauer, R.; Than, M. E.; Dobbek, H.; Gremer, L.; Melero, M.; Strobl, S.; Dias, J. M.; Soulimane, T.; Huber, R. A novel free-mounting system for protein crystals: Transformation and improvement of diffraction power by accurately controlled humidity changes. *J. Appl. Crystallogr.* **2000**, *33*, 1223–1230.
- (33) Sjogren, T.; Carlsson, G.; Larsson, G.; Hajdu, A.; Andersson, C.; Pettersson, H.; Hajdu, J. Protein crystallography in a vapour stream: Data collection, reaction initiation and intermediate trapping in naked hydrated protein crystals. *J. Appl. Crystallogr.* **2002**, *35*, 113–116.
- (34) Sanchez-Weatherby, J.; Bowler, M. W.; Huet, J.; Gobbo, A.; Felisaz, F.; Lavault, B.; Moya, R.; Kadlec, J.; Ravelli, R. B. G.; Cipriani, F. Improving diffraction by humidity control: A novel device compatible with X-ray beamlines. *Acta Crystallogr., Sect. D: Biol. Crystallogr.* **2009**, *65*, 1237–1246.
- (35) Hu, N. J.; Iwata, S.; Cameron, A. D.; Drew, D. Crystal structure of a bacterial homologue of the bile acid sodium symporter ASBT. *Nature* **2011**, *478*, 408–411.
- (36) Oliete, R.; Pous, J.; Rodriguez-Puente, S.; Abad-Zapatero, C.; Guasch, A. Elastic and inelastic diffraction changes upon variation of the relative humidity environment of PurE crystals. *Acta Crystallogr., Sect. D: Biol. Crystallogr.* **2013**, *69* (2), 194–212.
- (37) Malinauskaitė, L.; Quick, M.; Reinhard, L.; Lyons, J. A.; Yano, H.; Javitch, J. A.; Nissen, P. A mechanism for intracellular release of Na<sup>+</sup> by neurotransmitter/sodium symporters. *Nat. Struct. Mol. Biol.* **2014**, *21* (11), 1006–1012.
- (38) Hellmich, J.; Bommer, M.; Burkhardt, A.; Ibrahim, M.; Kern, J.; Meents, A.; Mühl, F.; Dobbek, H.; Zouni, A. Native-like Photosystem II Superstructure at 2.44 Å Resolution through Detergent Extraction from the Protein Crystal. *Structure* **2014**, *22* (11), 1607–1615.
- (39) de Sanctis, D.; Beteva, A.; Caserotto, H.; Dobias, F.; Gabadinho, J.; Giraud, T.; Gobbo, A.; Guijarro, M.; Lentini, M.; Lavault, B.; Mairs, T.; McSweeney, S.; Petitdemange, S.; Rey-Bakaiko, V.; Surr, J.; Theveneau, P.; Leonard, G. A.; Mueller-Dieckmann, C. ID29: A high-intensity highly automated ESRF beamline for macromolecular crystallography experiments exploiting anomalous scattering. *J. Synchrotron Radiat.* **2012**, *19* (3), 455–461.
- (40) Flot, D.; Mairs, T.; Giraud, T.; Guijarro, M.; Lesourd, M.; Rey, V.; van Brussel, D.; Morawe, C.; Borel, C.; Hignette, O.; Chavanne, J.; Nurizzo, D.; McSweeney, S.; Mitchell, E. The ID23-2 structural biology microfocus beamline at the ESRF. *J. Synchrotron Radiat.* **2010**, *17*, 107–118.
- (41) Nurizzo, D.; Mairs, T.; Guijarro, M.; Rey, V.; Meyer, J.; Fajardo, P.; Chavanne, J.; Biasci, J.-C.; McSweeney, S.; Mitchell, E. The ID23-1

- structural biology beamline at the ESRF. *J. Sync. Rad.* **2006**, *13* (3), 227–238.
- (42) Wakatsuki, S.; Belrhali, H.; Mitchell, E. P.; Burmeister, W. P.; McSweeney, S. M.; Kahn, R.; Bourgeois, D.; Yao, M.; Tomizaki, T.; Theveneau, P. ID14 Quadriga', a Beamline for Protein Crystallography at the ESRF. *J. Synchrotron Radiat.* **1998**, *5* (3), 215–221.
- (43) Brockhauser, S.; Svensson, O.; Bowler, M. W.; Nanao, M.; Gordon, E.; Leal, R. M.; Popov, A.; Gerring, M.; McCarthy, A. A.; Gotz, A. The use of workflows in the design and implementation of complex experiments in macromolecular crystallography. *Acta Crystallogr., Sect. D: Biol. Crystallogr.* **2012**, *68* (Pt 8), 975–84.
- (44) Gabadinho, J.; Beteva, A.; Guijarro, M.; Rey-Bakaikoa, V.; Spruce, D.; Bowler, M. W.; Brockhauser, S.; Flot, D.; Gordon, E. J.; Hall, D. R.; Lavault, B.; McCarthy, A. A.; McCarthy, J.; Mitchell, E.; Monaco, S.; Mueller-Dieckmann, C.; Nurizzo, D.; Ravelli, R. B. G.; Thibault, X.; Walsh, M. A.; Leonard, G. A.; McSweeney, S. M. MxCuBE: A synchrotron beamline control environment customized for macromolecular crystallography experiments. *J. Synchrotron Radiat.* **2010**, *17*, 700–707.
- (45) Incardona, M. F.; Bourenkov, G. P.; Levik, K.; Pieritz, R. A.; Popov, A. N.; Svensson, O. EDNA: A framework for plugin-based applications applied to X-ray experiment online data analysis. *J. Synchrotron Radiat.* **2009**, *16*, 872–879.
- (46) Sauter, N. K.; Grosse-Kunstleve, R. W.; Adams, P. D. Robust indexing for automatic data collection. *J. Appl. Crystallogr.* **2004**, *37* (3), 399–409.
- (47) Zhang, Z.; Sauter, N. K.; van den Bedem, H.; Snell, G.; Deacon, A. M. Automated diffraction image analysis and spot searching for high-throughput crystal screening. *J. Appl. Crystallogr.* **2006**, *39*, 112–119.
- (48) Powell, H. R.; Johnson, O.; Leslie, A. G. Autoindexing diffraction images with iMosflm. *Acta Crystallogr., Sect. D: Biol. Crystallogr.* **2013**, *69* (Pt 7), 1195–203.
- (49) Bourenkov, G. P.; Popov, A. N. Optimization of data collection taking radiation damage into account. *Acta Crystallogr., Sect. D: Biol. Crystallogr.* **2010**, *66*, 409–419.
- (50) Delagrière, S.; Brenchereau, P.; Launer, L.; Ashton, A. W.; Leal, R.; Veyrier, S.; Gabadinho, J.; Gordon, E. J.; Jones, S. D.; Levik, K. E.; McSweeney, S. M.; Monaco, S.; Nanao, M.; Spruce, D.; Svensson, O.; Walsh, M. A.; Leonard, G. A. ISPyB: An Information Management System for Synchrotron Macromolecular Crystallography. *Bioinformatics* **2011**, *27*, 3186–3192.
- (51) Mueller, U.; Darowski, N.; Fuchs, M. R.; Forster, R.; Hellmig, M.; Paithankar, K. S.; Puhringer, S.; Steffien, M.; Zocher, G.; Weiss, M. S. Facilities for macromolecular crystallography at the Helmholtz-Zentrum Berlin. *J. Synchrotron Radiat.* **2012**, *19* (Pt 3), 442–449.
- (52) Ursby, T.; Unge, J.; Appio, R.; Logan, D. T.; Fredslund, F.; Svensson, C.; Larsson, K.; Labrador, A.; Thunnissen, M. M. G. M. The macromolecular crystallography beamline I011-3 at the MAX IV laboratory. *J. Synchrotron Radiat.* **2013**, *20* (4), 648–653.
- (53) Larabi, A.; Devos, J. M.; Ng, S.-L.; Nanao, M. H.; Round, A.; Maniatis, T.; Panne, D. Crystal Structure and Mechanism of Activation of TANK-Binding Kinase 1. *Cell Rep.* **2013**, *3* (3), 734–746.
- (54) Pellegrini, E.; Piano, D.; Bowler, M. W. Direct cryocooling of naked crystals: Are cryoprotection agents always necessary? *Acta Crystallogr., Sect. D: Biol. Crystallogr.* **2011**, *67* (Pt 10), 902–906.
- (55) Wheeler, M. J.; Russi, S.; Bowler, M. G.; Bowler, M. W. Measurement of the equilibrium relative humidity for common precipitant concentrations: facilitating controlled dehydration experiments. *Acta Crystallogr., Sect. F: Struct. Biol. Cryst. Commun.* **2012**, *68* (Pt 1), 111–114.
- (56) Raoult, F.-M. *Acad. Sci., Paris, C. R.* **1887**, *104*, 1430–1433.
- (57) Flory, P. J. Thermodynamics of High Polymer-Solutions. *J. Chem. Phys.* **1942**, *10*, 51–61.
- (58) Flory, P. J. Fifteenth Spiers Memorial Lecture. Thermodynamics of polymer solutions. *Discuss. Faraday Soc.* **1970**, *49*, 7–29.
- (59) Huggins, M. L. Solutions of long chain compounds. *J. Chem. Phys.* **1941**, *9*, 440–440.
- (60) Sadeghi, R.; Shahebrahimi, Y. Vapor Pressure Osmometry Determination of Solvent Activities of Different Aqueous and Nonaqueous Polymer Solutions at 318.15 K. *J. Chem. Eng. Data* **2011**, *56* (6), 2946–2954.
- (61) Sadeghi, R.; Ziamajidi, F. Water activities of ternary mixtures of poly(ethylene glycol), NaCl and water over the temperature range of 293.15K to 313.15K. *J. Chem. Thermodyn.* **2006**, *38* (11), 1335–1343.
- (62) Eikenberry, E. F.; Brönnimann, C.; Hülsen, G.; Toyokawa, H.; Horisberger, R.; Schmitt, B.; Schulze-Briese, C. PILATUS: a two-dimensional X-ray detector for macromolecular crystallography. *Nuclear Instruments and Methods in Physics Research Section A: Accelerators, Spectrometers, Detectors and Associated Equipment* **2003**, *501* (1), 260–266.
- (63) Owen, R. L.; Axford, D.; Nettleship, J. E.; Owens, R. J.; Robinson, J. I.; Morgan, A. W.; Dore, A. S.; Lebon, G.; Tate, C. G.; Fry, E. E.; Ren, J.; Stuart, D. I.; Evans, G. outrunning free radicals in room-temperature macromolecular crystallography. *Acta Crystallogr., Sect. D: Biol. Crystallogr.* **2012**, *68* (7), 810–818.
- (64) Rajendran, C.; Dworkowski, F. S. N.; Wang, M.; Schulze-Briese, C. Radiation damage in room-temperature data acquisition with the PILATUS 6M pixel detector. *J. Synchrotron Radiat.* **2011**, *18* (3), 318–328.
- (65) Warkentin, M.; Badeau, R.; Hopkins, J.; Thorne, R. E. Dark progression reveals slow timescales for radiation damage between T = 180 and 240 K. *Acta Crystallogr., Sect. D: Biol. Crystallogr.* **2011**, *67* (9), 792–803.
- (66) Brockhauser, S.; Ravelli, R. B. G.; McCarthy, A. A. The use of a mini-kappa goniometer head in macromolecular crystallography diffraction experiments. *Acta Crystallogr., Sect. D: Biol. Crystallogr.* **2013**, *69* (7), 1241–1251.
- (67) Owen, R. L.; Pearson, A. R.; Meents, A.; Boehler, P.; Thominet, V.; Schulze-Briese, C. A new on-axis multimode spectrometer for the macromolecular crystallography beamlines of the Swiss Light Source. *J. Synchrotron Radiat.* **2009**, *16* (2), 173–182.
- (68) Royant, A.; Carpentier, P.; Ohana, J.; McGeehan, J.; Paetzold, B.; Noirclerc-Savoye, M.; Verneude, X.; Adam, V.; Bourgeois, D. Advances in spectroscopic methods for biological crystals. 1. Fluorescence lifetime measurements. *J. Appl. Crystallogr.* **2007**, *40* (6), 1105–1112.
- (69) Scherer, M.; Klingl, S.; Sevanna, M.; Otto, V.; Schilling, E. M.; et al. Crystal Structure of Cytomegalovirus IE1 Protein Reveals Targeting of TRIM Family Member PML via Coiled-Coil Interactions. *PLoS Pathog.* **2014**, DOI: 10.1371/journal.ppat.1004512.
- (70) Svensson, G.; Awad, W.; Hakansson, M.; Mani, K.; Logan, D. T. Crystal structure of N-glycosylated human glycan-1 core protein: Structure of two loops evolutionarily conserved in vertebrate glycan-1. *J. Biol. Chem.* **2012**, *287* (17), 14040–14051.
- (71) Strong, M.; Sawaya, M. R.; Wang, S.; Phillips, M.; Cascio, D.; Eisenberg, D. Toward the structural genomics of complexes: Crystal structure of a PE/PPE protein complex from Mycobacterium tuberculosis. *Proc. Natl. Acad. Sci. U. S. A.* **2006**, *103* (21), 8060–8065.
- (72) Awad, W.; Svensson Birkedal, G.; Thunnissen, M. M. G. M.; Mani, K.; Logan, D. T. Improvements in the order, isotropy and electron density of glycan-1 crystals by controlled dehydration. *Acta Crystallogr., Sect. D: Biol. Crystallogr.* **2013**, *69* (12), 2524–2533.
- (73) Hall, J. P.; O'Sullivan, K.; Naseer, A.; Smith, J. A.; Kelly, J. M.; Cardin, C. J. Structure determination of an intercalating ruthenium dipyridophenazine complex which kinks DNA by semiintercalation of a tetraazaphenanthrene ligand. *Proc. Natl. Acad. Sci. U. S. A.* **2011**, *108*, 17610–17614.
- (74) Hall, J. P.; Sanchez-Weatherby, J.; Alberti, C.; Quimper, C. H.; O'Sullivan, K.; Brazier, J. A.; Winter, G.; Sorensen, T.; Kelly, J. M.; Cardin, D. J.; Cardin, C. J. Controlled dehydration of a ruthenium complex–DNA crystal induces reversible DNA kinking. *J. Am. Chem. Soc.* **2014**, *136*, 17505–17512.
- (75) Berman, H. M.; Coimbatore Narayanan, B.; Di Costanzo, L.; Dutta, S.; Ghosh, S.; Hudson, B. P.; Lawson, C. L.; Peisach, E.; Prlic, A.; Rose, P. W.; Shao, C.; Yang, H.; Young, J.; Zardecki, C. Trendspotting in the Protein Data Bank. *FEBS Lett.* **2013**, *587* (8), 1036–1045.
- (76) Chruszcz, M.; Potrzebowski, W.; Zimmerman, M. D.; Grabowski, M.; Zheng, H.; Lasota, P.; Minor, W. Analysis of solvent content and

oligomeric states in protein crystals—Does symmetry matter? *Protein Sci.* **2008**, *17* (4), 623–632.

(77) Bowler, M. G.; Bowler, M. W. Measurement of the intrinsic variability within protein crystals: Implications for sample-evaluation and data-collection strategies. *Acta Crystallogr., Sect. F: Struct. Biol. Cryst. Commun.* **2014**, *70* (Pt 1), 127–132.

(78) Brejc, K.; van Dijk, W. J.; Klaassen, R. V.; Schuurmans, M.; van der Oost, J.; Smit, A. B.; Sixma, T. K. Crystal structure of an ACh-binding protein reveals the ligand-binding domain of nicotinic receptors. *Nature* **2001**, *411* (6835), 269–276.

(79) Li, J.; Edwards, P. C.; Burghammer, M.; Villa, C.; Schertler, G. F. X. Structure of Bovine Rhodopsin in a Trigonal Crystal Form. *J. Mol. Biol.* **2004**, *343* (5), 1409–1438.

(80) Lomakin, I. B.; Xiong, Y.; Steitz, T. A. The Crystal Structure of Yeast Fatty Acid Synthase, a Cellular Machine with Eight Active Sites Working Together. *Cell* **2007**, *129* (2), 319–332.

(81) Leal, R. M. F.; Bourenkov, G.; Russi, S.; Popov, A. N. A survey of global radiation damage to 15 different protein crystal types at room temperature: A new decay model. *J. Synchrotron Radiat.* **2013**, *20* (1), 14–22.

(82) Berger, M. A.; Decker, J. H.; Mathews, I. I. Diffraction study of protein crystals grown in cryoloops and micromounts. *J. Appl. Crystallogr.* **2010**, *43* (6), 1513–1518.

(83) Cipriani, F.; Rower, M.; Landret, C.; Zander, U.; Felisaz, F.; Marquez, J. A. CrystalDirect: A new method for automated crystal harvesting based on laser-induced photoablation of thin films. *Acta Crystallogr., Sect. D: Biol. Crystallogr.* **2012**, *68* (Pt 10), 1393–1399.

(84) Viola, R.; Carman, P.; Walsh, J.; Miller, E.; Benning, M.; Frankel, D.; McPherson, A.; Cudney, B.; Rupp, B. Operator-assisted harvesting of protein crystals using a universal micromanipulation robot. *J. Appl. Crystallogr.* **2007**, *40* (3), 539–545.

(85) Gati, C.; Bourenkov, G.; Klinge, M.; Rehders, D.; Stellato, F.; Oberthur, D.; Yefanov, O.; Sommer, B. P.; Mogk, S.; Duszenko, M.; Betzel, C.; Schneider, T. R.; Chapman, H. N.; Redecke, L. Serial crystallography on in vivo grown microcrystals using synchrotron radiation. *IUCrJ* **2014**, *1* (2), 87–94.